Structural singularities in GexTe100−x films

A. A. Piarristeguy, M. Micoulaut, R. Escalier, P. Jóvári, I. Kaban, J. van Eijk, J. Luckas, S. Ravindren, P. Boolchand, and A. Pradel

---

Articles you may be interested in

Structural singularities in Ge$_x$Te$_{100-x}$ films

A. A. Piarristeguy,[1] M. Micoulaut,[2] R. Escalier,[1] P. Jóvári,[3] I. Kaban,[4] J. van Eijk,[5] J. Luckas,[5] S. Ravindren,[6] P. Boolchand,[6] and A. Pradel[1]

[1]*Institut Charles Gerhardt, UMR 5253-CNRS, Case 1503, Université de Montpellier, Place Eugène Bataillon, 34095 Montpellier Cedex 5, France*
[2]*Laboratoire de Physique Théorique des Liquides, Université Pierre et Marie Curie, Boite 121, 4, Place Jussieu, 75252 Paris Cedex 05, France*
[3]*Wigner Research Center of Physics, Institute for Solid State Physics, H-1525 Budapest, Hungary*
[4]*IFW Dresden, Institute for Complex Materials, P.O. Box 27 01 16, D-01171 Dresden, Germany*
[5]*Physikalisches Institut (IA), RWTH Aachen University, 52056 Aachen, Germany*
[6]*School of Electronics and Computing Systems, College of Engineering and Applied Science, University of Cincinnati, Cincinnati, Ohio 45221-0030, USA*

Structural and calorimetric investigation of Ge$_x$Te$_{100-x}$ films over wide range of concentration $10 < x < 50$ led to evidence two structural singularities at $x \sim 22$ at. % and $x \sim 33$-35 at. %. Analysis of bond distribution, bond variability, and glass thermal stability led to conclude to the origin of the first singularity being the flexible/rigid transition proposed in the framework of rigidity model and the origin of the second one being the disappearance of the undercooled region resulting in amorphous materials with statistical distributions of bonds. While the first singularity signs the onset of the Ge–Ge homopolar bonds, the second is related to compositions where enhanced Ge–Ge correlations at intermediate lengthscales (7.7 Å) are observed. These two threshold compositions correspond to recently reported resistance drift threshold compositions, an important support for models pointing the breaking of homopolar Ge–Ge bonds as the main phenomenon behind the ageing of phase change materials. © *2015 AIP Publishing LLC.* [http://dx.doi.org/10.1063/1.4928504]

I. INTRODUCTION

Amorphous Ge-based chalcogenides have attracted considerable attention in recent decades due to their promising applications in both optics and optoelectronics.[1] Even though also investigated for the development of optical devices for far infrared photonic applications,[2,3] Ge-based tellurides were mainly studied for optoelectronics applications.[1] In particular, given the phase change applications of tellurides, used in optical discs such as CD-RW or DVD-RW discs or future nonvolatile memories, much effort is spent in the optimization of the functionalities which derive from their underlying physical properties. Present studies are devoted to the understanding of the limitations of the Te-based devices, some of which are crucial for a general improvement of, e.g., data storage performances. For instance, certain phase-change materials (PCMs) display phase separation phenomena[1,4] and stability problems during the production of the amorphous phase, which prevents from a sustainable phase switching over a large number of read-erase switching cycles.

On the other hand, in the domain of fundamental glass properties, amorphous germanium chalcogenides Ge-X (with X = S, Se, Te) represent attractive benchmark systems to test the validity of topological approaches of disordered materials, based on the notion of network rigidity.[5–7] According to rigidity theory, a certain number of compositional trends of physical and chemical properties, including the glass-forming ability itself, can indeed be understood from the inspection of the number of interatomic force-field constraints n_c arising from bond-stretching (BS) and bond-bending (BB) interactions. These interactions constrain the network structure at a molecular level in a mechanically effective way, and, ultimately, n_c can be compared to the available number of atomic degrees of freedom n_d per atom (3 in 3D). The condition $n_c = n_d = 3$ enunciated by Phillips[8] and identified with an optimal glass condition is nothing else than the isostatic stability criterion established by Lord Maxwell[9] for macroscopic structures and defines two classes of glassy materials. Networks having $n_c < 3$ are considered as "*flexible*" and contain internal deformation (floppy) modes as revealed by inelastic neutron scattering, while those having $n_c > 3$ are viewed to be overconstrained or "*stressed rigid*". Glasses with $n_c = 3$ are viewed to be isostatically rigid. Thorpe and co-workers[10,11] independently showed that the condition $n_c = 3$ coincides with a flexible to rigid elastic phase transition for which the control parameter is the network mean coordination number $\langle r \rangle$ and the order parameter of the transition is the density of floppy modes $f = 3 - n_c$. At the transition characterized by a critical coordination number of $\langle r \rangle = \langle r_c \rangle = 2.4$, the density of floppy modes vanishes and stressed rigidity onsets.

For a Ge$_x$S$_{100-x}$ or a Ge$_x$Se$_{100-x}$ glass, since Ge atom is 4-fold ($r = 4$), and the chalcogen X 2-fold coordinated ($r = 2$), the count of BS ($r/2$) and BB ($2r - 3$) mechanical constraints for Ge is 7 and for X is 2, so that the $n_c = 3$ (or $\langle r \rangle = 2.4$) condition is achieved when the Ge-atom content increases to $x = 20$ at. %.

In contrast with sulfides and selenides, it is not clear that tellurides always follow the 8-N rule (N being the outer

shell electrons). Several papers report evidence that tellurium has a coordination number slightly larger[12,13] than 2, and for the Ge atoms, one has $r_{Ge} \cong 4$.[14] Furthermore, it has been found that Ge is not only in tetrahedral sp^3 hybridized geometry but also in defect octahedral one.[13] The enumeration of angular constraints is therefore not straightforward. Based on an analysis using topological constraints of simulated Ge–Te glasses,[13,15] Micoulaut *et al.* proposed a way to calculate n_c. On this basis, it can be shown that a decrease of the tetrahedral fraction will increase the location of the flexible/rigid transition, while at the opposite, an increase of the Te coordination number will lower the threshold. Based on this work, Luckas *et al.*[16] evaluated the flexible/rigid transition at about 23 at. % Ge.

On the whole, while extensive investigations including structural, thermal, electrical, optical, mechanical characterization have been carried out on Ge sulfide and selenide glasses which exist in wide range of compositions, much less is known on the Ge–Te binary system which displays a reduced glass-forming region (GFR). As a matter of fact, bulk glass formation occurs in a narrow range of Ge concentration in the $15 < x < 22$ at. % range.[17,18] To circumvent the problem of the reduced GFR and investigate effects of Ge cross-linking over a large range in composition, we have used co-evaporation to produce films of about 7 μm in thickness.[14] In this way, the GFR was extended in the $12.0 \le x \le 45$ at. % range. The Ge_xTe_{100-x} films were recently characterized by high-energy X-ray diffraction (XRD), extended x-ray absorption fine structure (EXAFS), Reverse Monte Carlo (RMC) modeling, and thermal measurements.[14] A thorough investigation of these previous data helps in proposing new aspects of the structure of these materials.

II. EXPERIMENTAL DETAILS

A. Sample preparation

Ge_xTe_{100-x} films ($12.0 \le x \le 44.6$ at. %) were deposited by thermal co-evaporation using a MEB500 setup from PLASSYS.[18] Microscope slides were used as substrates and cleaned with alcohol and blow drying in air. Before a deposition, the chamber was evacuated down to 10^{-7} mbars in order to avoid ambient contamination. Ultra-pure tellurium powder (Goodfellow-99.999% and metallic impurities <200 ppm) was simultaneously evaporated from two heated sources, while ultra-pure germanium (Aldrich-99.999% and metallic impurities <200 ppm) chips were evaporated by electron-beam bombardment. During the deposition process, the substrate holder was rotated and heated to near 70 °C by using hot water circulation. The evaporation rate and thickness for each element were automatically controlled with pre-calibrated quartz crystal monitors.

An additional $Ge_{50}Te_{50}$ sample was prepared using DC magnetron sputtering from a stoichiometric GeTe target. Thin films with thickness between 1 and 3 μm were sputtered on Si-wafers coated with PMMA.

No further annealing treatment was carried out prior to characterization. The amorphous character of all as-deposited films was checked by X-ray diffraction using a PANalytical

XPERT diffractometer. A Cu ($k\alpha$) source was used for excitation ($\lambda = 1.5406$ Å). The compositions of co-evaporated films were checked by Electron Probe Micro-Analysis (EPMA) using a CAMECA SX-100 instrument with an acceleration voltage of 20 kV and probe current of 10 nA while the composition of the sputtered $Ge_{50}Te_{50}$ film was checked by energy dispersive X-ray spectroscopy.

The powders needed for the measurements were obtained by scratching the 7 μm-thick co-evaporated films deposited on glass substrates. In the case of the $Ge_{50}Te_{50}$ sputtered films, the amorphous material was first removed from the substrate by dissolving PMMA in acetone and the obtained flakes were then ground to a fine powder.

B. Measurements

The structure of six amorphous co-evaporated Ge_xTe_{100-x} films ($x = 12.0, 20.2, 24.1, 33.1, 36.8,$ and 44.6 at. %) and a sputtered $Ge_{50}Te_{50}$ film has been investigated by high-energy XRD at the BW5 wiggler beamline[19] of the DORIS III positron storage ring operated at the HASYLAB/DESY (Hamburg, Germany). EXAFS of the Ge and Te K-absorption edges was also performed on the six co-evaporated films at beamline X1 of Hasylab. See Ref. 14 for more details.

The thermal behaviour on amorphous Ge_xTe_{100-x} thick films ($11.6 \le x \le 48.0$ at. %) was investigated by Differential Scanning Calorimetry (DSC) using a Mettler DSC30. Around 8-10 mg of powder were put into aluminum pans. Continuous heating experiments were performed at 10 °C/min from room temperature to 450 °C.

C. RMC simulations

X-ray diffraction and EXAFS measurements of co-evaporated films were fitted simultaneously by the rmcpp code,[20] and simulation boxes contained 20 000 atoms. The number density of the samples was determined by interpolating the molar volumes of amorphous $Ge_{15}Te_{85}$[21] and $Ge_{50}Te_{50}$.[22] X-ray atomic form factors were taken from Ref. 23. EXAFS backscattering amplitudes and phases needed to calculate the model $\chi(k)$ function were obtained by the FEFF8.4 code.[24] It is to be mentioned that in conventional EXAFS analysis, broadening and asymmetric distribution of nearest neighbour distances are taken into account by cumulant expansion.[25,26] In RMC modeling, these quantities do not play a direct role as nearest neighbour distributions are represented by the first peak of the corresponding partial pair correlation functions.

The maximum random displacement of atoms in a move was 0.1 Å along each coordinate. The number of accepted moves was usually around 10^7. The minimum interatomic distance (cutoff) of Ge–Te and Te–Te pairs was 2.35 Å and 2.5 Å, respectively. The Ge–Ge cutoff was 2.25 Å in the runs where Ge–Ge bonding was allowed and 3.5 Å when Ge–Ge nearest neighbours were forbidden. In the constrained simulation runs, Ge atoms were forced to have 4 neighbours. This constraint was satisfied usually by more than 95% of Ge atoms. A full account of the RMC modelling technique and the description of basic structural results of the Ge–Te co-evaporated films can be found in Ref. 14.

III. RESULTS

A. Thermal properties

The glass transition temperatures T_g shown in Fig. 1 are found to vary linearly between $\approx 100\,°\text{C}$ and $200\,°\text{C}$ for compositions lower than 31 at. % Ge and are not observed anymore above this composition. The onset of the crystallization temperature T_x was found to display a linear increase between $140\,°\text{C}$ and $220\,°\text{C}$ for 22 at. % Ge, followed by a nearly plateau-like behavior, followed by a sharp decrease for compositions larger than 36 at. % Ge.

In the composition region where melt-quenched glasses can be obtained, the T_g values and even whole DSC plots of the co-evaporated samples are similar to those obtained by melt spinning[27] and twin roller quenching,[18] respectively. Therefore, these co-evaporated samples are not only amorphous materials but also glasses. More generally, the samples with composition lower than 31 at. % Ge which display T_g in their DSC plots will be considered as glasses. At the opposite, Ge-richer samples which do not exhibit any T_g are considered as amorphous materials.

The variation of T_g with composition can be well described using stochastic agglomeration theory[28,29] that leads to a parameter-free prediction of the T_g variation with composition (solid black line in Fig. 1),

$$T_g(x) - T_g(0) = \frac{T_g(0)}{\ln 2} x. \tag{1}$$

Here, we use $T_g(0) = 333$ K, a value similar to that found by others (340 K[30]).

The evolution of the onset of the crystallization temperature has been explained in Ref. 14. For the Te-rich glasses, two crystallization peaks are observed: the first one corresponding to Te crystallization appears at a temperature all the lower as the sample is rich in Te and the second one appears at ~220 °C whatever the Te content and corresponds to the crystallization of GeTe compound. For a Ge-content of 22 at. %, the two peaks merge and a single crystallization peak at about 220 °C

FIG. 2. (a) Total computed structure factor (circles) $S_{sim}(k)$ of amorphous $Ge_{36.8}Te_{63.2}$ compared to experimental data from X-ray diffraction (gray curve). (b) Experimental structure factors $S_{exp}(k)$ of amorphous $Ge_x Te_{100-x}$ films with $12.0 \leq x \leq 50$ at. %.

is observed for the Ge-richer samples up to a composition of 35 at. % in Ge when the onset of the crystallization starts decreasing abruptly.

B. Structure factor and decomposition

Figure 2(a) shows a typical total computed structure factor $S_{sim}(k)$, obtained from a linear combination of the partial structure factors $S_{ij}(k)$, for amorphous $Ge_{36.8}Te_{63.2}$.

Among the studied compositions, one (20 at. % Ge) prepared by conventional melt-quenching has already been investigated by X-ray diffraction.[31] The obtained structure factors for both materials prepared by melt-quenched and co-evaporation technique are similar as reported earlier in Ref. 14, which conforts the findings of thermal investigation indicating that our materials are very similar to conventional glasses.
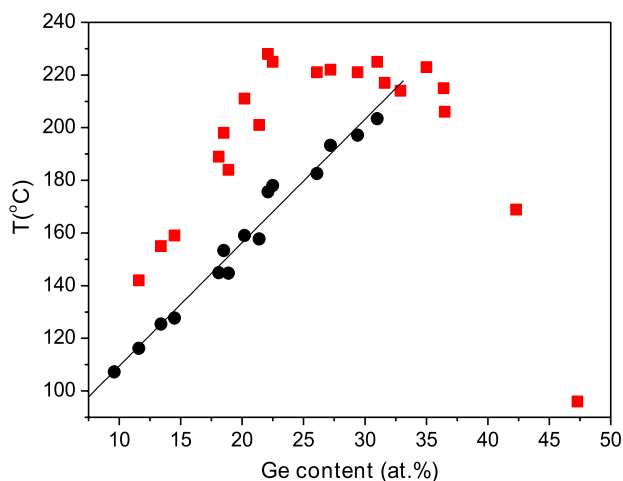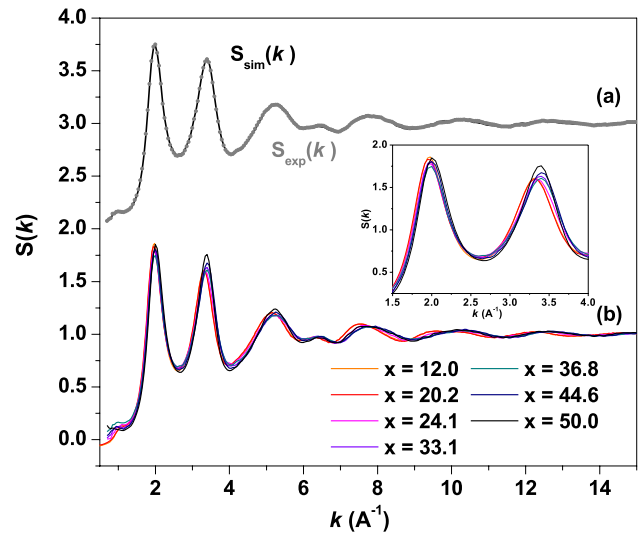

FIG. 1. Glass transition temperature T_g (black circles) and onset of the crystallization temperature T_x (red squares) behavior with Ge content in $Ge_x Te_{100-x}$ amorphous films. The solid black line is a prediction using stochastic agglomeration theory.[28,29]
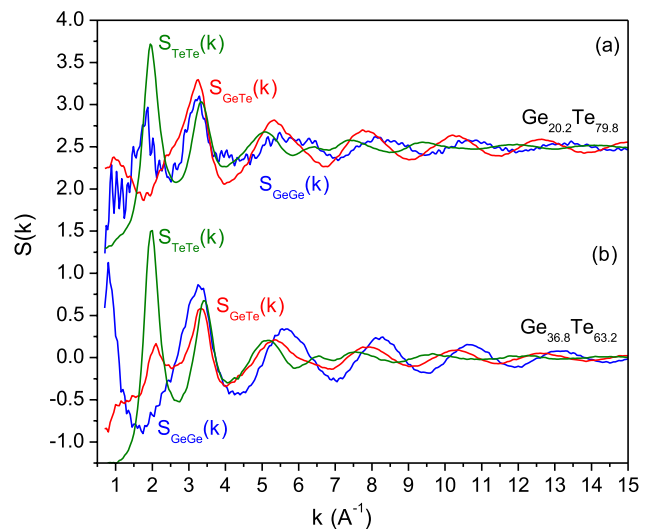

FIG. 3. Decomposition into partial structure factors $S_{GeTe}(k)$ (red lines), $S_{GeGe}(k)$ (blue lines), and $S_{TeTe}(k)$ (green lines) for (a) $Ge_{20.2}Te_{79.8}$ and (b) $Ge_{36.8}Te_{63.2}$.

As seen from Fig. 2, the computed $S_{sim}(k)$ reproduces very well the X-ray diffraction results[14] ($S_{exp}(k)$) in all studied k-range. The presence of intermediate range order (IRO) manifests by the existence of a First Sharp Diffraction Peak (FSDP) located at a wavevector of $k_{FSDP} \approx 1.0$-1.1 Å^{-1}. In the high wavevector range ($k < 9$ Å^{-1}), five wider oscillations can also be identified that are usually associated with the short range order (SRO) of the amorphous state. The first principal peak (PP) is found at 1.95-2.00 Å^{-1} and does not depend much on composition, whereas the second PP shifts to higher wavevector from 3.33 Å^{-1} to 3.40 Å^{-1} (see Fig. 2(b)).

A decomposition into partial structure factors (Figs. 3(a) and 3(b)) clearly indicates the contribution of $S_{GeTe}(k)$, $S_{GeGe}(k)$, and $S_{TeTe}(k)$ to different peaks for amorphous Ge$_{20.2}$Te$_{79.8}$ and Ge$_{36.8}$Te$_{63.2}$. The most relevant results in the partial structure factors $S_{ij}(k)$ are observed for the FSDP

($k_{FSDP} \approx 1$ Å^{-1}) and the first principal peak ($k_1 \approx 1.95$ Å^{-1}). Figure 4 shows the three partial contributions $S_{GeTe}(k)$, $S_{GeGe}(k)$, and $S_{TeTe}(k)$ for all studied amorphous films. Obviously, there is no contribution from $S_{TeTe}(k)$ to the FSDP of the total structure factor, so that the FSDP is mostly due to contributions from Ge–Te (Fig. 4(a)) and Ge–Ge (Fig. 4(b)). For both, an important dependence with Ge content is obtained, and it can furthermore be noticed that the non-monotonic evolution of the FSDP with x defines two regions in compositions. Indeed, for Te-rich compositions ($12.0 \leq x \leq 24.1$ at. %), the FSDP at ≈ 1.0 Å^{-1} appears to result only from $S_{GeTe}(k)$. Similarly, we find that in $S_{GeGe}(k)$, there is a clear separation between compositions in the ($12.0 \leq x \leq 24.1$ at. %) range and those studied in the ($33.1 \leq x \leq 50.0$ at. %) range, which indicate that at higher Ge, typical Ge–Ge correlations have built up in reciprocal space and give rise to a FSDP. One also remarks that the PP at $k \approx 1.9$ Å^{-1} displays the opposite behavior and has nearly vanished at high Ge content.

C. Signature from Bhatia-Thornton structure factors

Figs. 3 and 4 show that the FSDP is dominated for the $S_{GeTe}(k)$ in three Ge-poor compositions ($x = 12.0, 20.2, 24.1$ at. %) whereas $S_{GeGe}(k)$ mostly contributes for four Ge-rich compositions ($x = 33.1, 36.8, 44.6, 50.0$ at. %). These results suggest some kind of structural rearrangement on an intermediate lengthscale to occur in the $24.1 < x < 33.1$ at. % range. These can be quantified using Bhatia-Thornton concentration-concentration partial structure factors $S_{CC}(k)$ involving long-range concentration-concentration correlations[32–34] as shown in Fig. 5. All functions exhibit a principal peak at ≈ 2 Å^{-1} that builds up with increasing Ge content, and in the high wavevector region, $S_{CC}(k)$ converges to the limit $c_{Ge}c_{Te} = x(1 - x)$ which is a direct consequence of the definition,[35]
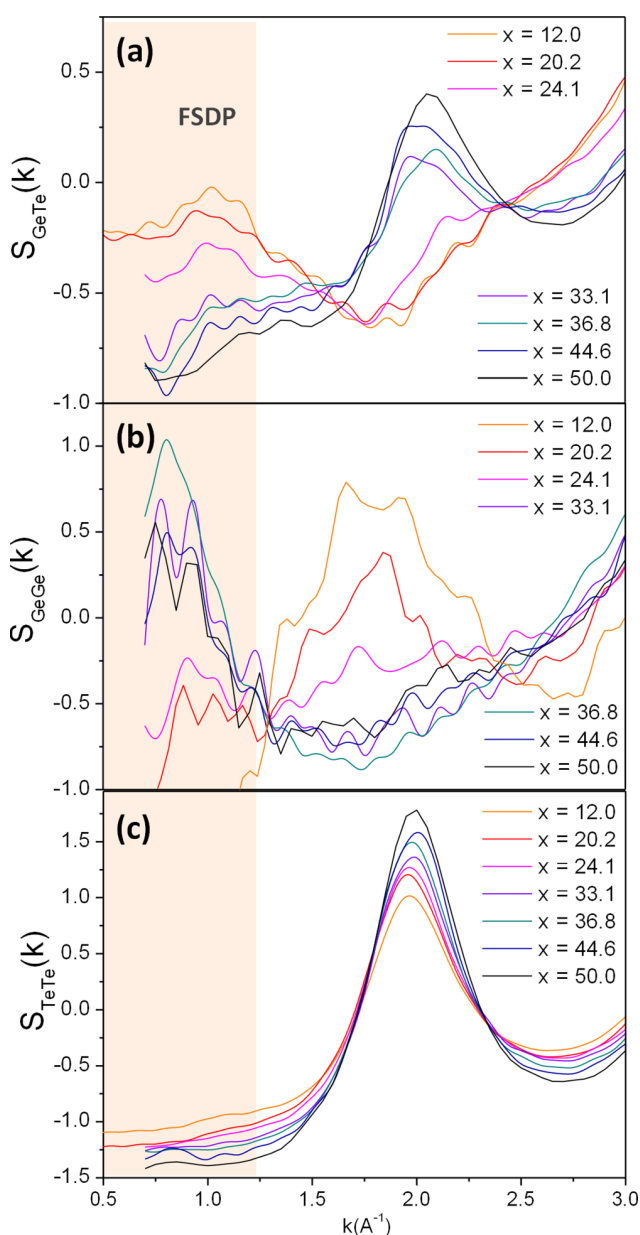

FIG. 4. Computed partial structure factors $S_{GeTe}(k)$ (a), $S_{GeGe}(k)$ (b), and $S_{TeTe}(k)$ (c) in amorphous Ge$_x$Te$_{100-x}$ films. The approximate FSDP region (light orange) is indicated.
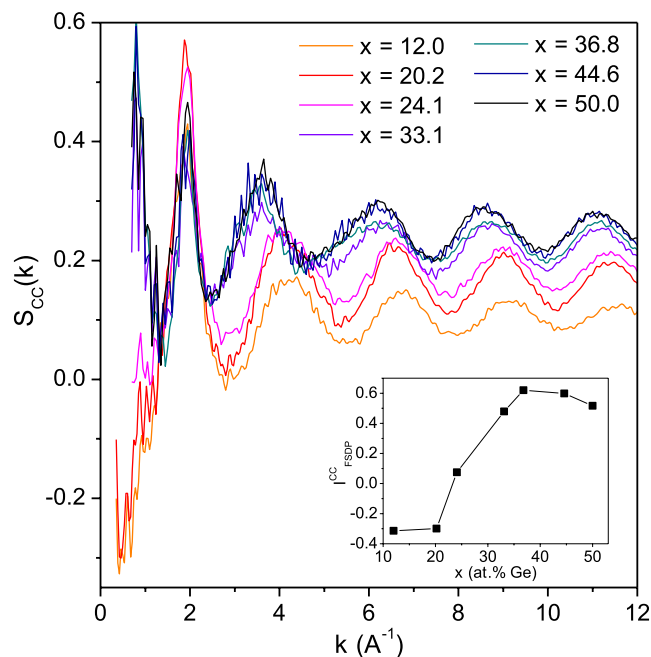

FIG. 5. Calculated Bhatia-Thornton concentration-concentration structure factor $S_{CC}(k)$ in amorphous Ge$_x$Te$_{100-x}$ films. The inset shows the intensity of the pre-peak found at ≈ 1 Å^{-1} as a function of composition.

$$S_{CC}(k) = c_{Ge}c_{Te}\left[1 + S_{GeGe}(k) + S_{TeTe}(k) - 2S_{GeTe}(k)\right], \quad (2)$$

where $S_{GeGe}(k)$, $S_{GeTe}(k)$, and $S_{TeTe}(k)$ are the Faber-Ziman structure factors (Fig. 4) which follow the limit $S_{ij}(k) \rightarrow 1$ for large k. We note that the oscillations of $S_{CC}(k)$ in Fig. 5 with respect to the limit $c_{Ge}c_{Te}$ have a smaller amplitude in the telluride rich film ($x = 12$). This indicates a smaller tendency to have Ge–Ge or Te–Te correlations at low x, and one can therefore conclude that the structure is made of a random mixing of Ge atoms into the base Te-rich network. Interestingly, the function $S_{CC}(k)$ also exhibits a FSDP in the region 0.9-1.0 Å^{-1} which shows marked changes with Ge composition as highlighted in the inset of Fig. 5. The intensity of the FSDP increases indeed abruptly between the 24.1 and the 33.1 at. % compositions, and for the Ge-rich compositions, an intense FSDP peak is obtained. The typical distances involved can be roughly determined from the position of the FSDP (≈ 1 Å^{-1}) that is associated with some repetitive characteristic distance between Ge atoms involving a lengthscale[36] for concentration-concentration correlations of $7.7/k_{\text{FSDP}} = 7.7$ Å.

D. Pair correlations and decomposition

In real space, Figs. 6 and 7 show the experimental total pair correlation functions and computed partial pair correlation functions for the Ge–Te films, respectively. The experimental data show the presence of three domains of compositions corresponding to three different shifts in the position of the first main peak (2.68 Å for $x = 12.0$ and 20.2; 2.62 Å for $x = 24.1$; and 2.58 Å for $x = 33.1$, 36.8, 44.6, and 50.0). Two peaks are found in Ge–Ge and Te–Te partials at respective distances of 2.45 Å and 2.73 Å, and these are related to homopolar Ge–Ge and Te–Te bonds, respectively (Fig. 7). Their evolution is, obviously, related to the Ge content, and Ge–Ge bonds are absent for the 12.0 at. % composition. However, a small fraction is found for the 20.2 at. % composition which leads to a small peak at ≈ 2.45 Å and this peak is found to increase upon further Ge addition. On the opposite, the Te–Te peak is the dominant feature for the Te-rich films, and its intensity decreases with
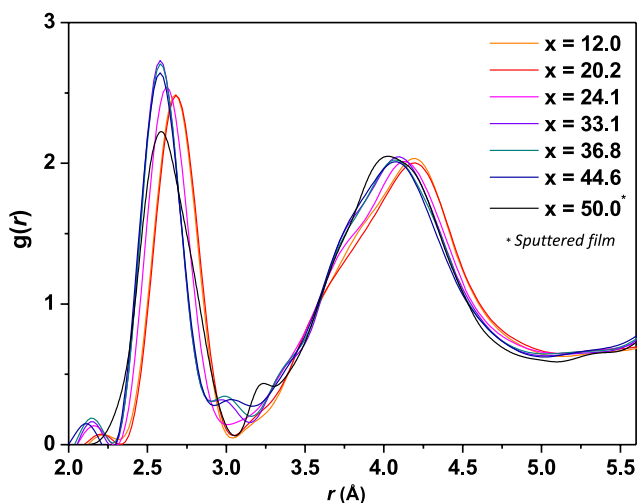
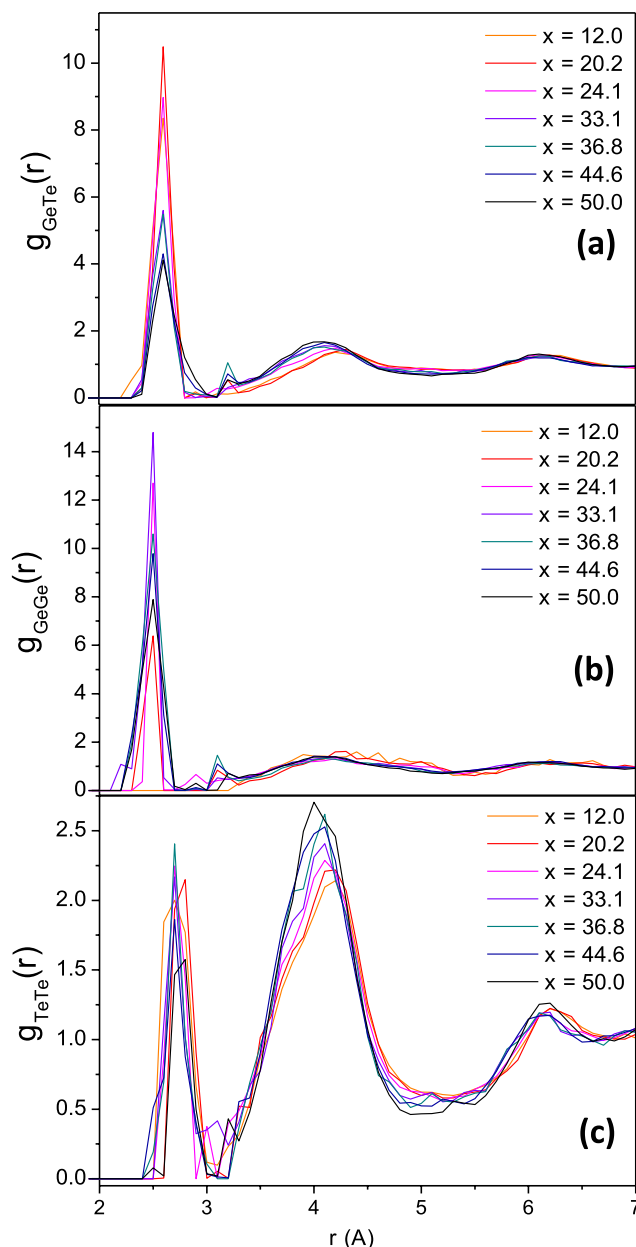FIG. 7. Partial pair correlation functions of RMC models of amorphous Ge$_x$Te$_{100-x}$ films.

FIG. 6. Experimental pair correlation functions of amorphous Ge$_x$Te$_{100-x}$ films.

x. The widths and heights of the first PP of each partial correlation functions $g_{GeTe}(r)$ (≈ 2.60 Å), $g_{GeGe}(r)$ (≈ 2.45 Å), and $g_{TeTe}(r)$ (≈ 2.73 Å) have been computed. The widths represented in Fig. 8(a) were extracted from Gaussian fittings of the functions $g_{ij}(r)$, allowing for an estimate of a full width at half maximum (FWHM) σ, and the evolution with Ge content was established with respect to the composition having the narrowest width, i.e., we followed $W(x) = (\sigma(x) - \sigma_{\text{ref}})/\sigma_{\text{ref}}$ with Ge content. The heights are represented in Fig. 8(b). The evolution of the $g_{GeGe}(r)$ parameters displays the most obvious features. Two singularities are observed: the first one between 20 and 25 at. % when the Ge–Ge bonds start appearing and the second one at about 35 and 37 at. % when the width of $g_{GeGe}(r)$ suddenly increases while its height decreases. The evolutions of $g_{GeTe}(r)$ and $g_{TeTe}(r)$ parameters follow the same trend with the presence of the two singularities.
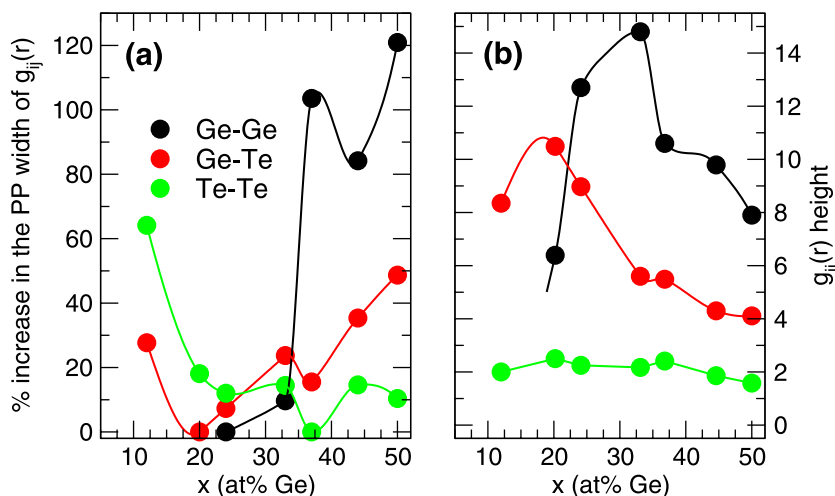
FIG. 8. Widths (a) and heights (b) of the first peak in partial correlation functions $g_{TeTe}(r)$ (green), $g_{GeTe}(r)$ (red), and $g_{GeGe}(r)$ (black) as a function of Ge content in amorphous Ge_xTe_{100-x} films.

E. Bond statistics

Using the structure fitted by RMC, we can calculate the statistics of bonds as a function of composition. Fig. 9 displays the total computed fraction of homopolar bonds (Ge–Ge and Te–Te, see detail in the inset). As observed in the figure, significant numbers of homopolar Ge–Ge and Te–Te bonds are obtained for nearly all samples (except the 12.0 at. % one), including for the Te-rich (for Ge–Ge) and Ge-rich ones (for Te–Te), indicating that the degree of resiliency of such bonds exceeds by far what can be imposed by chemical ordering. Te–Te bonds are present in all studied compositions and exhibit a decrease with Ge content, whereas Ge–Ge bonds appear at about 20 at. % Ge (Fig. 7(b)). Interestingly, when followed with Ge content, the total fraction of homopolar bonds goes through a minimum for 20-25 at. % Ge. Since both statistics are related, the minimum in homopolar bonds implies that the fraction of heteropolar Ge–Te bonds will pass through a maximum in the same compositional interval of 20-25 at. % Ge. Saturation in the number of total homopolar bonds occurs at a composition of 33 at. % Ge.

IV. DISCUSSION

Two structural singularities at $x \sim 22$ at. % Ge and ~33-35 at. % Ge have been detected from the analysis of XRD and EXAFS data of Ge_xTe_{100-x} films coupled to RMC modeling (Figs. 5-9). In the following, attempt to get a deeper insight into these singularities will be described.

A. Bonds

The singularities have signatures in the distribution of different bonds, i.e., heteropolar Ge–Te ones and homopolar Ge–Ge and Te–Te ones, as evidenced in Figure 9. The most striking feature at the composition of the first singularity at ~22 at. % Ge is the onset of the first Ge–Ge homopolar bonds. Interestingly enough, and even though it results from the two opposite trends of Ge–Ge and Te–Te bonds (inset of Fig. 9), at the same time, the general tendency is to form a network where heteropolar bonds are maximized. A constant distribution of heteropolar/homopolar bonds is observed for the Ge-rich materials above the second singularity at ~33-35 at. % Ge.

Figure 8 reports on the evolution of widths and heights of the principal peak of the pair correlation functions $g_{GeTe}(r)$, $g_{GeGe}(r)$, and $g_{TeTe}(r)$. The width of the principal peak is a direct measure of the bond variability of the amorphous network, i.e., neighbor distributions contributing to the PP and having a similar mean will lead to a sharp peak in the corresponding partial pair correlation function. Alternatively, if the nearest neighbor bonds are not well defined, one will have a large bond variability (or bond mismatch with respect to the equilibrium value) and the spread will lead to a broad principal peak. The width in the $g_{ij}(r)$ is a measure of the distance dispersion for each type of bond (Ge–Te, Ge–Ge, and Te–Te). In other words, a very narrow width of the Gaussian peak indicates that the distances between two atoms are almost the same in the sample.

Having these basic statements in hand, we can now analyze in more detail the results on the width of the PP. For the Te–Te partial (green curve in Fig. 8), Te-rich compositions
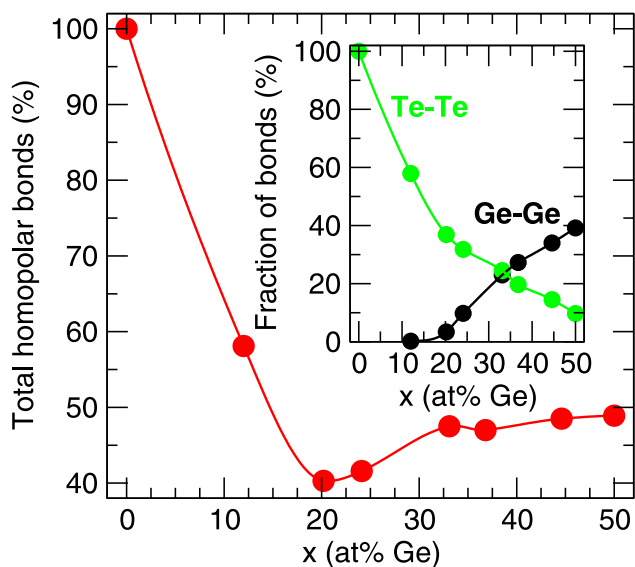

FIG. 9. Simulated RMC fraction of total homopolar bonds in amorphous Ge_xTe_{100-x} films. The inset shows the contribution of Ge–Ge (black) and Te–Te bonds (green).

lead to larger variations for the first neighbor bond distances, and these induce an increase of about 65% of the PP width, as compared to the reference 20.2 at. % sample. For Ge-richer compositions, the variations become smaller. On the other hand, Ge–Ge pairs, absent for $x < 20$ at. %, first exhibit small variations for the first neighbor bond distances and then show a sudden increase of the PP width for $x > 33$ at. %. The width of the PP of the Ge–Te pairs decreases from the $x = 12.0$ at. % composition to a minimum value for the 20.2 at. % sample and then increases back again.

The most striking feature in Figure 8 is the sudden and huge increase of the Ge–Ge pairs width for $x > 33$ at. %. In this Ge-rich region, the Ge–Te bond variability is also large. Such a result is consistent with a structure showing a large local disorder. As a matter of fact, it has been shown that a completely random model could be used to fit the structural data in the Ge-rich region above 33 at. %.[14] A statistical distribution of bonds is also consistent with the roughly constant distribution of bonds observed in the same region (Figure 9) and to the constant FSDP (I_{cc}) of the concentration-concentration structure factor $S_{CC}(k)$ (inset in Fig. 5).

In the region below 33 at. % Ge, the bond variability trends can be explained by the flexible or rigid nature of the system. As long as the system is flexible (Te-rich, $x < 22$ at. %), there are local deformation modes which allow the system to experience a variety of radial excursions which are frozen at the glass transition. As a result, bond will exhibit larger bond variability in flexible networks, and corresponding widths of the PP of the functions $g_{ij}(r)$ will be larger. For Ge-rich compositions ($22 < x < 33$ at. %), the density of cross-links imposes an increased tendency of bonds to adapt under stress, resulting also in larger bond variability. This feature is consistent with the well-known relationship between stressed rigidity and bond mismatch in simple bond networks,[37] revealing that atoms with a given coordination number cannot fulfill all their bonds at the same length because of a too high bond density or network connectivity.

Figures 8 and 9 are consistent for a flexible/rigid transition to occur at $x \sim 22$ at. % when the heteropolar content is maximum and the bond variability minimum.

B. Thermal stability

The two singularities have also signatures in the thermal properties of the materials as seen in Figure 1.

The first one at ~20 at. % Ge occurs when the two crystallization peaks merge. At this composition, the crystallization first controlled exclusively by tellurium starts being controlled also by germanium. It is also at the place where the glass stability measured by the temperature difference $\Delta T = T_x - T_g$ is maximum.[14]

The second singularity takes place at the composition where the materials do not exhibit T_g anymore and the crystallization temperature starts decreasing abruptly. It is consistent with the findings of structural investigation indicating that the materials possess a completely random structure with statistical distributions of bonds.

While a change from an exclusive control of crystallization by Te to a control by Ge can be understood by the onset of

Ge–Ge bonds at $x \sim 22$ at. % Ge, a maximized thermal stability at this composition cannot be understood on this basis.

In the early work of rigidity theory, it has been stated that glasses displaying $n_c = 3$ are "*optimal glasses*", i.e., glasses which form easily from a melt quench and are stable against thermal excitations.[8] Alternatively, such "*optimal glasses*" also manifest by an increased tendency to delay recrystallization upon heating.[38] As a result, the quantity $\Delta T = T_x - T_g$ reveals a measure of thermal stability of glasses, and a maximum indicates an indirect signature of the "*optimal glass*" as exemplified for various chalcogenide glasses.[39–42]

So, our data point towards the transition from flexible to rigid glasses to occur at a composition of ~22 at. % Ge in the Ge–Te system.

C. Summary—comparison with lighter chalcogenides

The two singularities at ~22 at. % and ~33-35 at. % Ge have signatures in both thermal and structural properties of Ge$_x$Te$_{100-x}$ films.

While the main feature of the first singularity is the onset of first homopolar Ge–Ge bonds, several other features point towards an optimal glass (in the sense of Phillips[8]) to be obtained at the singularity composition. For example, a maximum in ΔT and therefore an increased thermal stability of the glass are observed. The better structural ordering of this composition (maximized heteropolar bonds and lower dispersion in bond lengths) is also consistent with the idea of an optimal glass. These characteristics lead us to propose that the flexible/rigid transition in Ge$_x$Te$_{100-x}$ glasses occur at the composition ~22 at. % Ge. The onset of Ge–Ge bondings would appear when the glass becomes too rigid to accommodate all Ge atoms in a pure heteropolar environment. Then, it would be essentially a consequence of the flexible/rigid transition.

The origin of the second singularity lies in the strong tendency of Ge$_x$Te$_{100-x}$ materials to crystallize. It occurs at the composition ~33 at. % Ge where no undercooled liquid can be obtained due the merging of T_g and T_x. In this case, the structural investigation indicates that the co-evaporated Ge$_x$Te$_{100-x}$ films have a completely random structure with a statistical distribution of bonds and very high local disorder.

The situation in lighter Ge-S and Ge-Se chalcogenides is somewhat different. It is not so surprising owing to the known differences between the two families of materials, such an ease in obtaining glasses over wide composition ranges, chemically ordered structures with Ge in pure tetrahedral environment and pure two-fold coordination for tellurium in the case of the light chalcogenides.

The onset of the Ge–Ge homopolar bonds occurs at different compositions for tellurides and for sulfides and selenides, i.e., at ~22 at. % Ge and at ~33 at. % Ge, respectively. In the last case, it is consistent with the chemically ordered structure adopted by light chalcogenide glasses. As a result, the Ge–Se bond fraction steadily increases with Ge content up to the composition of the chemical threshold, i.e., 33 at. % Ge. This chemical threshold is supposed to be linked with the presence of stable stoichiometric compositions of 33 at. % Ge that can be associated with the existing crystalline polymorphs GeSe$_2$[43] and GeS$_2$.[44] The situation is different in tellurides since only

one stable crystalline polymorph has been reported to exist in the Ge–Te phase diagram and it corresponds to a composition of 50 at. % Ge (c-GeTe[45]). In the selenide system, the existence of heterogeneous glasses for $x > 33$ has been proposed on the basis of a series of experiments including thermal, mechanical, optical, Raman and Mossbauer measurements[46–49] by Boolchand on one hand and more recently by Yang *et al.*[50] on the other.

While the transition from a flexible to rigid network at ~22 at. % Ge has an important effect in tellurides with the onset of homopolar Ge–Ge bonds, it leads to slight signatures in sulfides and selenides. It is mainly tracked through thermal measurements. For example, a minimum in the activation energy for enthalpy relaxation for $\langle r \rangle = 2.4$ (20 at. % Ge) is attributed to such transition in germanium selenide glasses by Lucas *et al.*[51] Investigation on the basis of modulated differential scanning calorimetry experiments led Boolchand to propose the existence of the transition over a range of compositions, leading to the concept of intermediate phase.[52,53]

D. Link with resistance drift phenomena

The present findings have important implications for the field of PCMs. One major limitation of PCMs is related to the stability of data storage and the ageing phenomena that give rise to a loss with time in the electrical contrast between the amorphous and crystalline phases. Ageing process is related to an increase of the amorphous state resistivity after amorphization that usually follows a power law of the form,

$$\rho(t) = \rho_o \left(\frac{t - t'}{t_o} \right)^{\alpha}, \qquad (3)$$

where the parameter ρ_o denotes the resistivity at time to, i.e., $\rho(t_o) = \rho_o$ and to the time span between material elaboration and the start of the drift measurement. The drift parameter α determines the change in resistivity, the higher the value of α, the stronger the resistance drift.

Recently, it has been shown[16] that the same families of Ge–Te films as the ones studied here but elaborated in a different way (co-sputtering) exhibit for $x < 25$ at. % (i.e., flexible glasses) a continuous decrease of the drift parameter α with decreasing Ge content. This indicates a reduced tendency to ageing. For stressed rigid Ge–Te alloys ($26 < x < 50$ at. % Ge), the drift parameter α first leads to rather high values (typically, $\alpha = 0.29$) for compositions between 25 and 35 at. % Ge and then decreases abruptly for larger Ge content. The two observed thresholds can be traced back to the present findings signaling a rigidity transition at ~22 at. % Ge corresponding also to the onset of Ge–Ge bonds, and evidence for enhanced Ge–Ge correlations at intermediate lengthscales at ~33 at. %. We can, thus, conclude that the obtained correlations between resistance drift threshold compositions[16] and the threshold compositions detected from a structural analysis indicate the central role played by the presence of Ge–Ge correlations, both in real space and reciprocal space, in the ageing of PCMs. Their evolution as a function of Ge content appears to be a key-point for further understanding[54,55] and material optimization.

V. CONCLUSIONS

Thermal and structural measurements on Ge_xTe_{100-x} films in combination with RMC modelling have been carried out. Two structural singularities were observed. The first one at ~22 at. % Ge which coincides with the onset of the first homopolar Ge–Ge bonds displays characteristics compatible with the flexible/rigid transition identified in the rigidity theory, such as maximized heteropolar bonds, lowest bond variability, and maximized thermal stability. Huge Ge-related bond variability and evidence for enhanced Ge–Ge correlations at intermediate lengthscales are observed in the Ge-rich region starting above the second singularity at ~33-35 at. % Ge. It is linked to the disappearance of T_g and increased tendency to crystallization at this composition. In this Ge-rich region, materials possess a completely random structure with statistical distributions of bonds. The two thresholds coincide with thresholds recently reported to exist in the evolution of resistive drift coefficients in similar Ge_xTe_{100-x} films, i.e., with the ageing phenomena in these films. Therefore, the present findings have important implications for the field of phase change materials. To date improvements related to stability of data storage and the ageing phenomena have been derived from studies of selected compositions/systems only, and therefore, general concepts and results such as those found in the present Ge–Te films may provide an increased guidance for such compositionally related studies.

[1]M. Wuttig, Nat. Mater. **4**, 265 (2005).
[2]C. Vigreux, E. Barthelemy, L. Bastard, J. E. Broquin, M. Barillot, S. Menard, G. Parent, and A. Pradel, Opt. Lett. **36**(15), 2922 (2011).
[3]P. Lucas, Z. Y. Yang, M. K. Fah, T. Luo, S. B. Jiang, C. Boussard-Pledel, M. L. Anne, and B. Bureau, Opt. Mater. Express **3**, 1049 (2013).
[4]*Phase Change Materials and Applications*, edited by S. Raoux and M. Wuttig (Springer, Berlin, 2008).
[5]*Rigidity Theory and Applications*, edited by M. F. Thorpe and P. M. Duxbury (Kluwer Academic, Plenum Publishers, New York, 1999).
[6]*Phase Transitions and Self-organization in Electronic and Molecular Networks*, edited by M. F. Thorpe and J. C. Phillips (Kluwer Academic, Plenum Publishers, New York, 2001).
[7]*Rigidity and Boolchand Phases in Nanomaterials*, edited by M. Micoulaut and M. Popescu (INOE Publishing House, Bucarest, 2009).
[8]J. C. Phillips, J. Non-Cryst. Solids **34**, 153 (1979).
[9]J. C. Maxwell, Philos. Mag. **27**, 294 (1864).
[10]M. F. Thorpe, J. Non-Cryst. Solids **57**, 355 (1983).
[11]H. He and M. F. Thorpe, Phys. Rev. Lett. **54**, 2107 (1985).
[12]A. Menelle, R. Bellissent, and A. M. Flanck, Europhys. Lett. **4**, 705 (1987).
[13]M. Micoulaut, K. Gunasekera, S. Ravindren, and P. Boolchand, Phys. Rev. **90**, 094207 (2014).
[14]P. Jóvári, A. Piarristeguy, R. Escalier, I. Kaban, J. Bednarcik, and A. Pradel, J. Phys.: Condens. Matter **25**, 195401 (2013).
[15]K. Gunasekera, P. Boolchand, and M. Micoulaut, J. Appl. Phys. **115**, 164905 (2014).

[16]J. Luckas, A. Olk, P. Jost, J. Alvarez, A. Jaffré, P. Zalden, A. Piarristeguy, A. Pradel, C. Longeaud, and M. Wuttig, Appl. Phys. Lett. **105**, 092108 (2014).

[17]M. Popescu, *Non-Crystalline Chalcogenides* (Kluwer, Academic Press, New York, 2000).

[18]A. A. Piarristeguy, E. Barthélémy, M. Krbal, J. Frayret, C. Vigreux, and A. Pradel, J. Non-Cryst. Solids **355**, 2088 (2009).

[19]R. Bouchard, D. Hupfeld, T. Lippmann, J. Neuefeind, H. B. Neumann, H. F. Poulsen, U. Rütt, T. Schmidt, J. R. Schneider, J. Süssenbach, and M. von Zimmermann, J. Synchrotron Radiat. **5**, 90 (1998).

[20]O. Gereben, P. Jóvári, L. Temleitner, and L. Pusztai, J. Optoelectron. Adv. Mater. **9**, 3021 (2007).

[21]J. Kalikka, J. Akola, R. O. Jones, S. Kohara, and T. Usuki, J. Phys.: Condens. Matter **24**, 015802 (2012).

[22]S. Kohara, K. Kato, S. Kimura, H. Tanaka, T. Usuki, and K. Suzuya, Appl. Phys. Lett. **89**, 201910 (2006).

[23]D. Waasmaier and A. Kirfel, Acta Crystallogr., Sect. A: Found. Crystallogr. **51**, 416 (1994).

[24]A. L. Ankudinov, B. Ravel, J. J. Rehr, and S. D. Conradson, Phys. Rev. B **58**, 7565 (1998).

[25]J. J. Rehr and R. C. Albers, Rev. Mod. Phys. **72**, 621 (2000).

[26]G. Dalba, P. Fornasini, R. Grisenti, and J. Purans, Phys. Rev. Lett. **82**, 4240 (1999).

[27]I. Kaban, E. Dost, and W. Hoyer, J. Alloys Compd. **379**, 166 (2004).

[28]G. G. Naumis, Phys. Rev. B **73**, 172202 (2006).

[29]M. Micoulaut, Eur. Phys. J. B **1**, 277 (1998).

[30]D. Derewnicka, P. Zielinski, and H. Davies, J. Mater. Sci. Lett. **1**, 87 (1982).

[31]L. Rétkai, A. P. Goncalves, G. Delaizir, C. Godart, I. Kaban, B. Beuneu, and P. Jóvári, Solid State Commun. **151**, 1524 (2011).

[32]P. S. Salmon, J. Non-Cryst. Solids **353**, 2959 (2007).

[33]P. S. Salmon, R. A. Martin, P. E. Mason, and G. Cuello, Nature **435**, 75 (2005).

[34]C. Massobrio and A. Pasquarello, Phys. Rev. B **75**, 014206 (2007).

[35]H. E. Fischer, A. C. Barnes, and P. S. Salmon, Rep. Prog. Phys. **69**, 233 (2006).

[36]We relate the position r of a peak in real space to the position k of a corresponding peak in Fourier space by using the relation $k^*r \approx 7.7$, which identifies the location of the first maximum of the spherical Bessel function $j_0(kr)$. See P. S. Salmon, Proc. R. Soc. A **445**, 351 (1994).

[37]N. Mousseau and M. F. Thorpe, Phys. Rev. B **52**, 2660 (1995).

[38]A. Inoue, *Bulk Amorphous Alloys: Preparation and Fundamental Characteristics* (Trans Tech Publications, Zurich, 1998), p. 2.

[39]G. S. Varma, C. Das, and S. Asokan, Solid State Commun. **177**, 108 (2014).

[40]S. R. Gunti and S. Asokan, J. Appl. Phys. **111**, 033518 (2012).

[41]S. R. Gunti and S. Asokan, J. Non-Cryst. Solids **356**, 1637 (2010).

[42]P. Pattanayak and S. Asokan, J. Non-Cryst. Solids **354**, 3824 (2008).

[43]Y. Wang, M. Nakamura, O. Matsuda, K. Inoue, and K. Murase, J. Non-Cryst. Solids **198-200**, 753 (1996).

[44]V. G. Dittmar and H. Schäfer, Acta Crystallogr., Sect. B: Struct. Crystallogr. Cryst. Chem. **31**, 2060 (1975).

[45]S. Raoux, W. Welnic, and D. Ielmini, Chem. Rev. **110**, 240 (2010).

[46]S. Mamedov, D. G. Georgiev, T. Qu, and P. Boolchand, J. Phys.: Condens. Matter **15**, S2397 (2003).

[47]L. Cai and P. Boolchand, Philos. Mag. B **82**, 1649 (2002).

[48]P. Boolchand, P. Chen, M. Jin, B. Goodman, and W. J. Bresser, Physica B **389**, 18 (2007).

[49]P. Boolchand, D. G. Georgiev, T. Qu, F. Wang, L. Cai, and S. Chakravarty, C. R. Chim. **5**, 713 (2002).

[50]G. Yang, Y. Gueguen, J.-C. Sangleboeuf, T. Rouxel, C. Boussard-Plédel, J. Troles, P. Lucas, and B. Bureau, J. Non-Cryst. Solids **377**, 54 (2013).

[51]P. Lucas, E. A. King, O. Gulbiten, J. L. Yarger, E. Soignard, and B. Bureau, Phys. Rev. B **80**, 214114 (2009).

[52]S. Bhosle, P. Boolchand, M. Micoulaut, and C. Massobrio, Solid State Commun. **151**, 1851 (2011).

[53]S. Chakraborty and P. Boolchand, J. Phys. Chem. B **118**, 2249 (2014).

[54]K. V. Mitrofanov, A. V. Kolobov, P. Fons, X. Wang, J. Tominaga, Y. Tamenori, T. Uruga, N. Ciocchini, and D. Ielmini, J. Appl. Phys. **115**, 173501 (2014).

[55]A. V. Kolobov, P. Fons, and J. Tominaga, Phys. Rev. B **87**, 155204 (2013).